Supporting Information

Conflicting Interfacial Electrostatic Interactions as a Design Principle to Modulate Long-Range Inter-Domain Communication

Adithi Kannan, Dhruv Kumar Chaurasiya & Athi N. Naganathan*

[1]Department of Biotechnology, Bhupat & Jyoti Mehta School of Biosciences, Indian Institute of Technology Madras, Chennai 600036, India.

AUTHOR INFORMATION

Corresponding Author

e-mail: athi@iitm.ac.in

Phone: +91-44-2257 4140

Table S1 The RMSD matrix (in Å) between the conformational susbstates sampled by MD simulations and reported in Figure 6I of the main text.

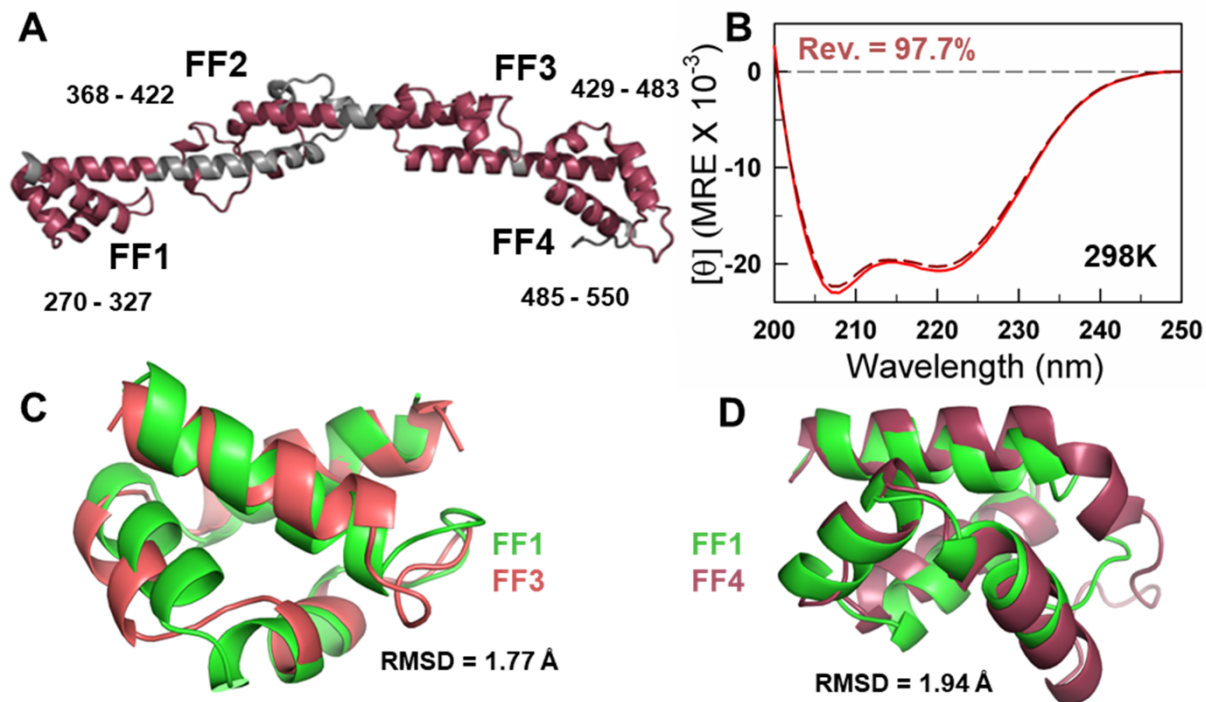| Time	0 μs	0.93 μs (a)	2.47 μs (b)	3.62 μs (c)	4.40 μs (d)	4.74 μs (e)
0 μs	-	6.1	8.0	8.0	12.9	7.2
0.93 μs (a)	6.1	-	6.6	7.7	12.7	7.4
2.47 μs (b)	8.0	6.6	-	7.2	9.1	7.8
3.62 μs (c)	8.0	7.7	7.2	-	11.1	3.8
4.40 μs (d)	12.9	12.7	9.1	11.1	-	11.6
4.74 μs (e)	7.2	7.4	7.8	3.8	11.6	-

Figure S1 (A) The AlphaFold2-predicted structure of p190A FF1-4 tandem repeats. The pink and gray regions represent the FF domains and the inter-domain linker, respectively. (B) The far-UV CD spectrum of FF34 recorded at 298 K prior (solid line) and post-temperature ramping (dashed line) shows high reversibility of the protein at a low concentration. (C, D) Structure alignment of FF3 (panel C) and FF4 (panel D) with the NMR-solved structure of FF1 (PDB: 2k85).
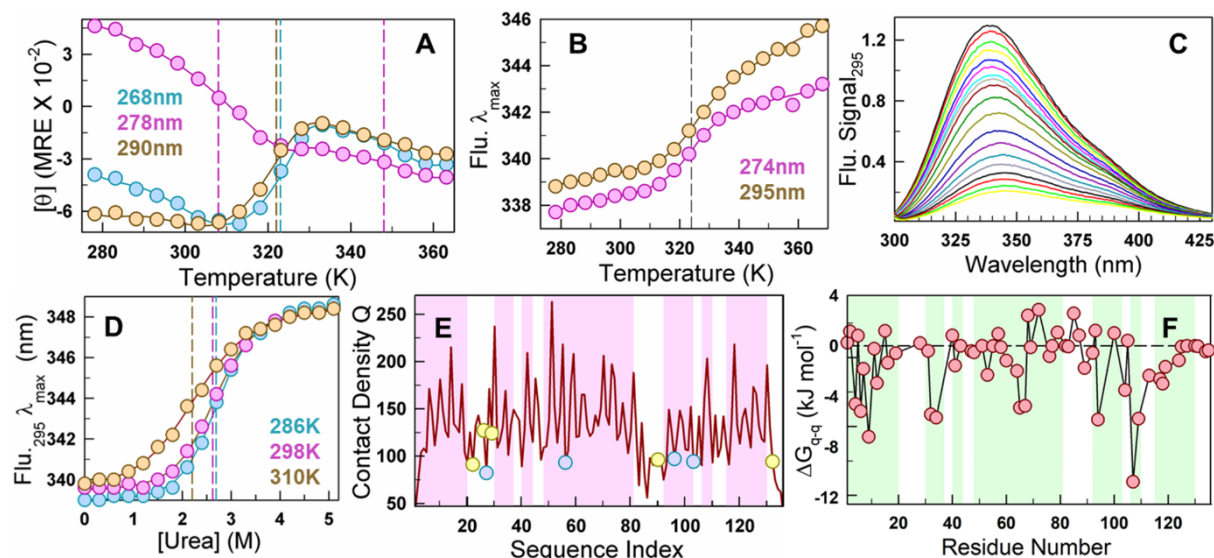
Figure S2 (A) The thermal denaturation curves of the WT monitored at 268 nm (cyan), 278 nm (magenta) and 290 nm (orange) in the near-UV CD experiment. The thermal melts at 278 nm and 290nm are also shown in the main text as Figure 2C. (B) The fluorescence emission maximum wavelength of FF34 WT upon excitation of protein at 274 nm (magenta) and 295 nm (orange). (C) The fluorescence emission spectrum obtained as a function of temperature upon excitation at 295nm. (D) The emission maximum wavelength from fluorescence measurements as a function of urea recorded at three temperatures — 286 K (cyan), 298 K (magenta) and 310 K (orange). The vertical dashed lines in panels A, B and D represent the inflection point. (E) The contact density with a cut-off of 5 Å represented against the sequence index. The yellow and the cyan circles represent the proline and glycine residues, respectively. (F) The Tanford-Kirkwood (TK) electrostatic interaction free energies as a function of sequence index. The shaded regions in panels E and F represent the helical regions.
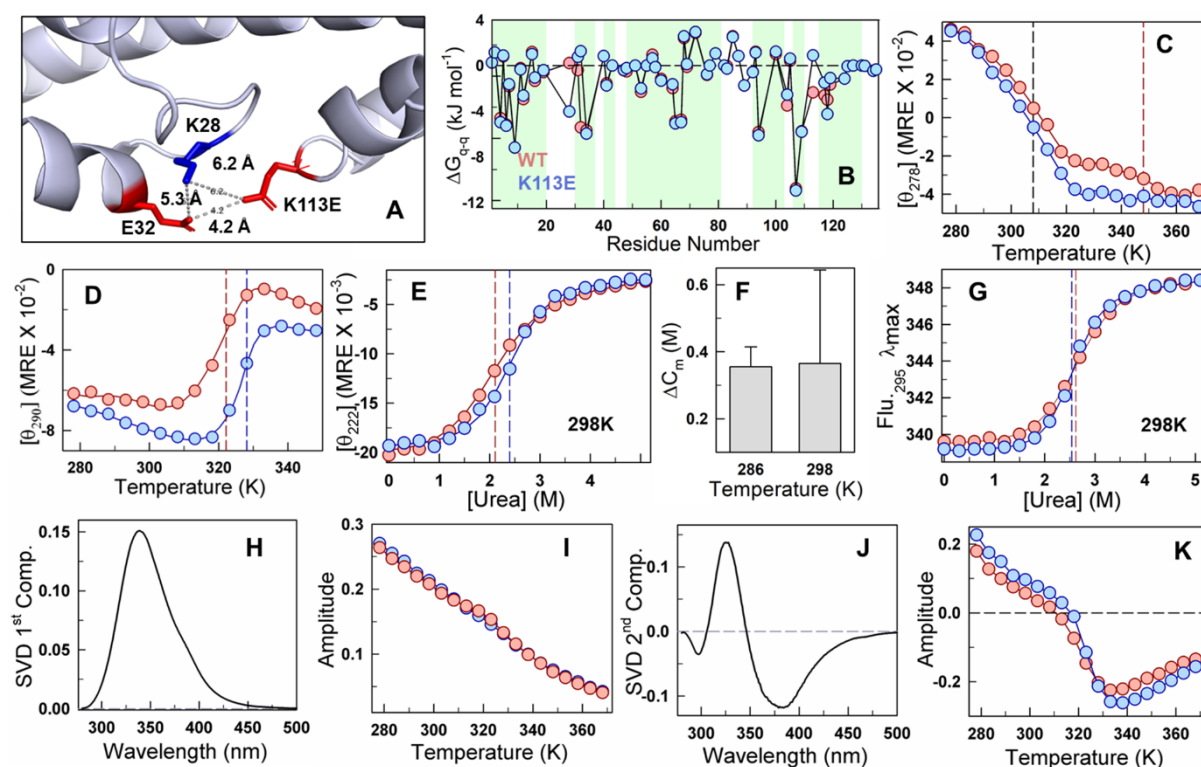
Figure S3 (A) The interface of FF34 K113E mutant with the pairwise distances depicted between the corresponding *troika* residues (sticks). (B) The TK interaction free energies of FF34 WT (red) and K113E mutant (blue) show minimal changes in the trends, except in the interface region (around K28 and K/E113 residues). (C, D) The near-UV CD thermal melting curve obtained by monitoring 278 nm (panel C) and 290 nm (panel D) for the WT and the mutant. The vertical dashed lines indicate the inflection point. Note that the inflection point (~308K) of the first unfolding stage in panel C is the same for the WT and mutant. The dashed line at ~348 K corresponds to only the WT, due to the absence of any second unfolding stage in the mutant. (E) The chemical denaturation curves obtained from far-UV CD measurements at 222 nm and 298 K for both constructs and (F) the difference in chemical denaturation midpoints ($\Delta C_{m,\ mutant} - \Delta C_{m,WT}$) at 286 K and 298 K show the higher stability of the K113E mutant. (G) The urea-dependent melting curves obtained from the fluorescence emission maximum wavelength show changes in cooperativity but little changes in stability. (H, I) The first component of SVD analysis of the fluorescence measurements at 274 nm excitation (panel H) and its corresponding temperature-dependent amplitudes (panel I). (J, K) The second component of SVD analysis of the fluorescence measurements (panel J) and the corresponding temperature-dependent amplitudes (panel K).
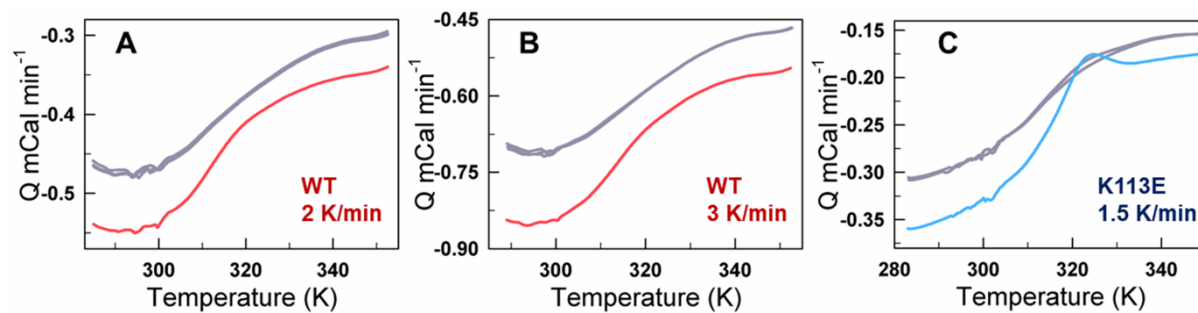
Figure S4 The raw heat capacity profiles of the WT recorded at a scan rate of (A) 2 K min^{-1} and (B) 3 K min^{-1} and (C) the K113E mutant recorded at 1.5 K min^{-1}. The concentration of both constructs was ~44 μM. The protein scans are shown in color, while the gray curves represent the buffer.

A MRNERKRVEMRRAFKENLETSPFITPGKPWEEARSFIMNEDFYQW
LEESVYMDIYGKHQKQIIDKAKEEFQELLLEYSELFYELELDAKPS
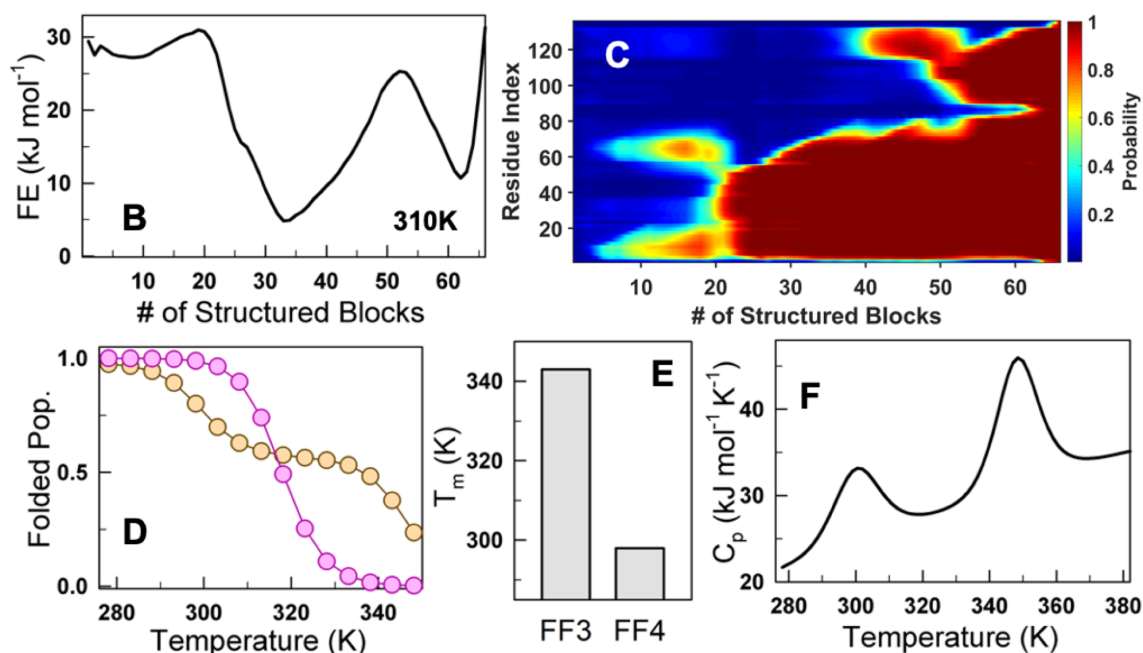KEKMGVIQDVLGEEQRFKALQKLQAERDALILKHIHFVYHPTKET

Figure S5 *Predictions from the uncalibrated Wako−Saitô−Muñoz−Eaton (WSME) model.* (A) Pictorial representation of the blocks mapped onto the FF34 sequence. Black and red represent adjacent blocks. (B) One-dimensional free energy profile resembles a three-state-like folding mechanism. (C) Residue folding probability as a function of the reaction coordinate signals an earlier folding of N-terminal subdomain similar to the prediction in the calibrated model (Figure 5 in the main text). (D, E) The folded population trends as a function of temperature (panel D) and the melting temperature of FF3 and FF4 from the uncalibrated model (panel E). The orange circles represent the model-predicted folded population showing an uncoupled unfolding event of the subdomains. The magenta circles represent the data from far-UV CD experiments. The uncalibrated model also predicts higher stability for the FF3 subdomain. (F) The predicted DSC curve of FF34 WT with two separate peaks, highlighting the earlier unfolding of FF4 (the first transition), followed by FF3 (the second transition).
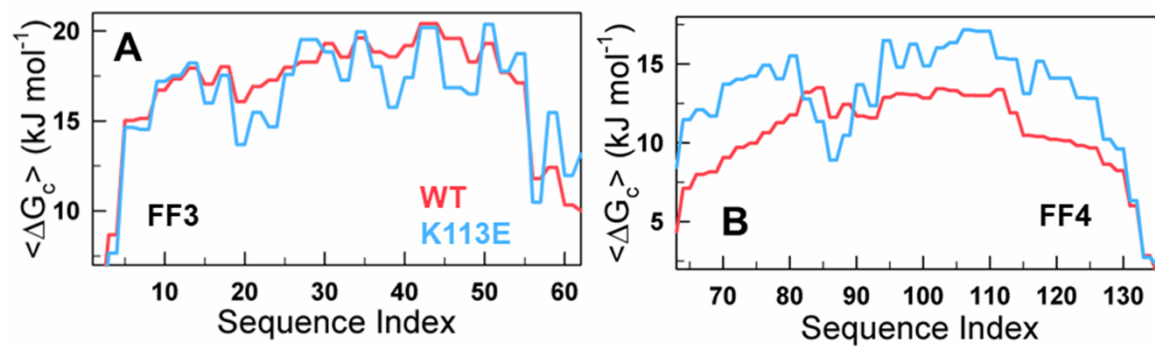
Figure S6 (A, B) The intradomain thermodynamic coupling free energies predicted from the calibrated WSME model for FF3 (panel A) and FF4 (panel B). The red and blue lines in the panels represent the WT and the K113E mutant, respectively.
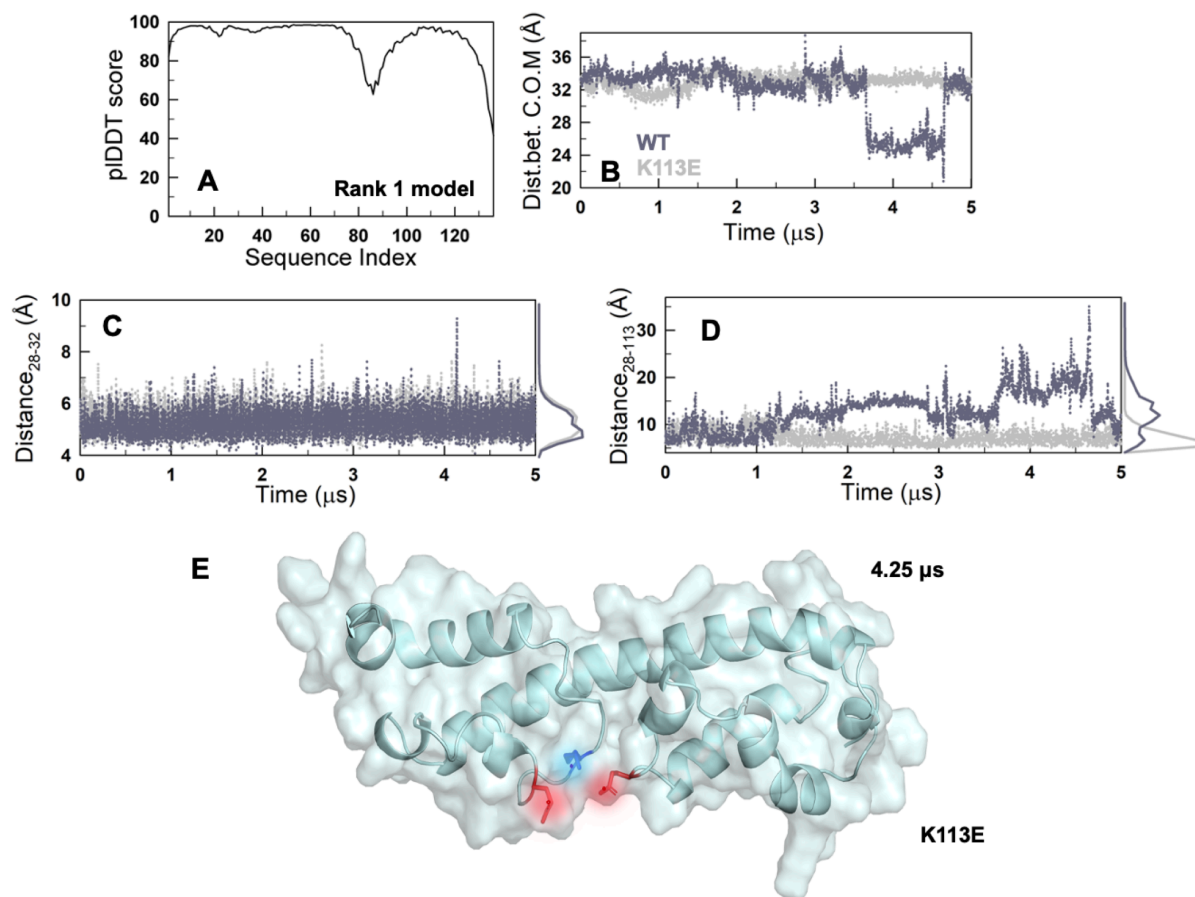
Figure S7 (A) The pLDDT score of the AlphaFold2-ColabFold predicted model (rank 1) of FF34 shows similar trends to the RMSF of the mutant calculated from MD simulations (Figure 6B in the main text). (B) The distance between the centre of mass of the FF3 and FF4 subdomains (calculated form the backbone atoms alone) for both constructs. A drastic relative movement is observed only in the WT. (C, D) The distance between the *troika* residues K28-E32 (panel C) and K28-K/E113 (panel D). The former pair remains close for both constructs. On the other hand, the distance between the subdomains as monitored by K28 and K113 in the WT (dark gray) shows large fluctuations with time. (E) The MD simulation snapshot of the mutant at 4.25 μs corresponding to a representative conformation sampled according to the principal component analysis.
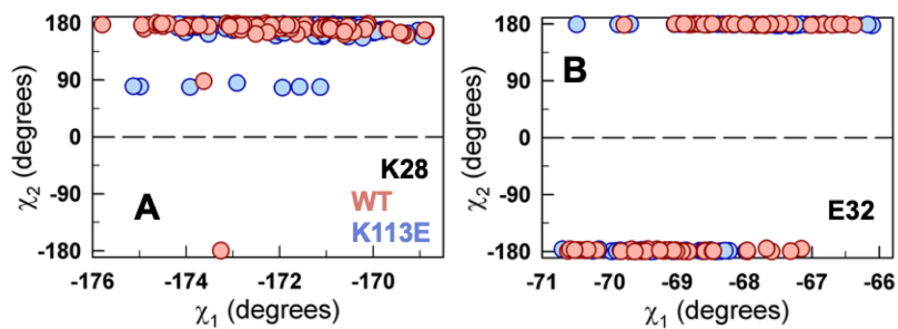
Figure S8 (A, B) The χ_1 and χ_2 rotameric dihedral angles of residues K28 (panel A) and E32 (panel B) of the WT (red) and the mutant (blue) calculated from the 80 AlphaFold2-ColabFold predicted structures of each construct.
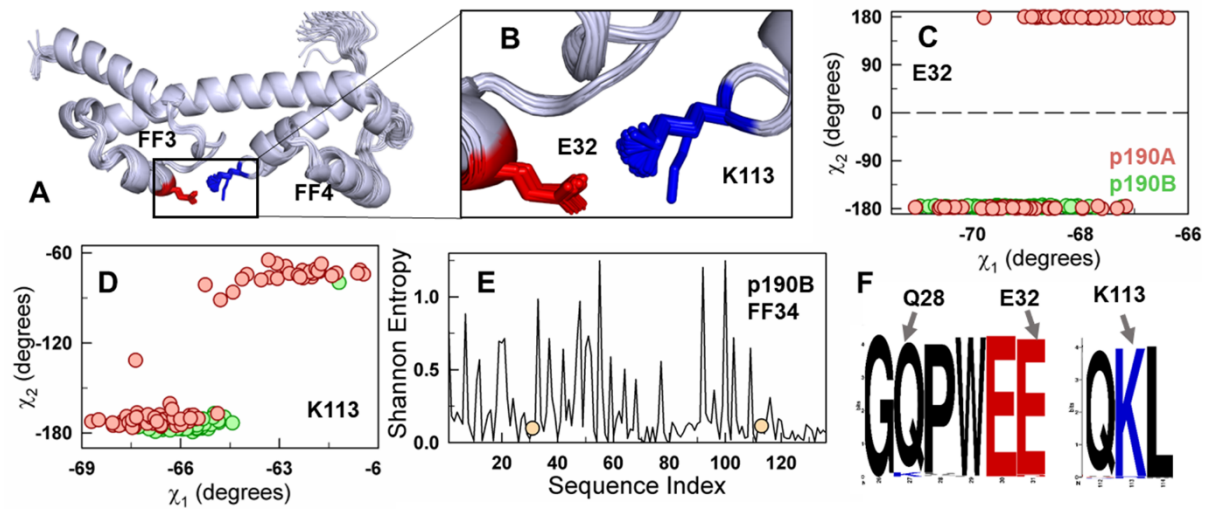
Figure S9 (A, B) Superimposition of 80 AlphaFold2-ColabFold predicted structures of p190B RhoGAP FF34 (ARHGAP5 gene, panel A) with the interface charge residues depicted in sticks (panel B). (C, D) The χ_1 and χ_2 rotameric dihedral angle of the residue E32 (panel C) and K113 (panel D) show a unimodal distribution of the χ_2 angle for p190B (green), in contrast to p190A (red). (D) Shannon entropy as a function of sequence index for p190B obtained from the multiple sequence alignment (MSA) of p190B FF34 orthologs. The orange circles represent the residues in p190B corresponding to two of the *troika* residues (E32, K113) in p190A FF34. (E) The sequence logo obtained from the MSA of p190B orthologs shows that the nature of the amino acid at the interface corresponding to residues 28, 32 and 113 remains conserved.
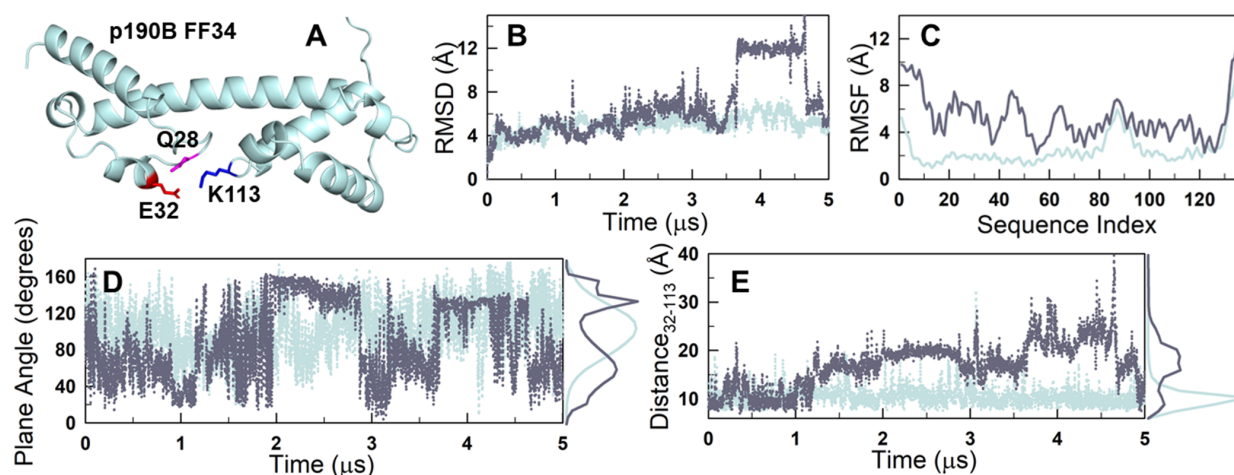
Figure S10 *p190B FF34 that does not harbor the charge troika exhibits minimal dynamics.* (A) The AlphaFold2-ColabFold predicted structure of p190B FF34. The three equivalent residues in p190B FF34 - Q28, E32 and K113 - corresponding to the charge *troika* in p190A FF34 are shown in magenta, red and blue sticks, respectively. (B-E) The root-mean-squared deviation (panel B), the root-mean-squared fluctuations (panel C), the plane angle (refer to the main text; panel D), and the distance between the center of mass of residue 32 and 113 (located in FF3 and FF4, respectively; panel E) of p190A FF34 (dark gray) and p190B FF34 (pale cyan).